Exploration of BioMat-X

Open Exploration

Open Access Original Article

A tri-layer tissue engineering heart valve scaffold based on atelocollagen, hyaluronic acid, and elastin

Zhaoying Ma[1*], Robin J. Scales[1], David D. Brand[2], Jan T. Czernuszka[1]

[1]Department of Materials, University of Oxford, OX13PH Oxford, UK
[2]Collagen Research Core, Memphis Veterans Affairs Medical Centre's Research Service, Memphis, TN 38163, USA

***Correspondence:** Zhaoying Ma, Department of Materials, University of Oxford, OX13PH Oxford, UK. zhaoying.ma@materials.ox.ac.uk

Academic Editor: Ajay Vikram Singh, German Federal Institute for Risk Assessment (BfR), Germany
Received: April 16, 2024 **Accepted:** August 26, 2024 **Published:** August 29, 2024

Cite this article: Ma Z, Scales RJ, Brand DD, Czernuszka JT. A tri-layer tissue engineering heart valve scaffold based on atelocollagen, hyaluronic acid, and elastin. Explor BioMat-X. 2024;1:215–30. https://doi.org/10.37349/ebmx.2024.00016

Abstract

Aim: This study aims to fabricate and characterise a novel tri-layer scaffold based on type I atelocollagen, hyaluronic acid (HA), and a novel fibrillar elastin gel, mimicking the native heart valve leaflets in structure, composition, and mechanical properties, among which, the bending anisotropic behaviour in both the with curvature (WC) and the against curvature (AC) directions, is the most desired. The use of atelocollagen is of significant importance in highlighting the non-antigenic potential of the design.

Methods: Porous scaffolds were freeze-dried, then crosslinked using 1-ethyl-3-(3-dimethylaminopropyl)carbodiimide (EDC) and *N*-hydroxysuccinimide (NHS). The fibrillogenesis occurrence and the scaffold microstructure were imaged using scanning electron microscopy (SEM). Fourier transform infrared spectroscopy (FITR) investigated the effect of fabrication and crosslinking on the backbone structure. Dynamic mechanical analysis (DMA) characterised the compressive and bending properties of the scaffolds in hydrated and non-hydrated states. Three-point bending and a "self-deflection" test were performed on tri-layer scaffolds in both WC and AC directions.

Results: Atelocollagen-based scaffolds were successfully produced, rendering this study the first to report a tri-layer structure using atelocollagen, HA, and elastin fibrillar gel. The scaffolds' porosity was tailored to accommodate potential future biological studies and the transition between layers appeared seamless. FITR unveiled effective crosslinking and the backbone structure preservation. The scaffolds exhibited lightly crosslinked polymer resembling mechanical responses when non-hydrated, and the desired J-curve stress-strain response was observed when hydrated. The tri-layer scaffolds showed anisotropic bending behaviour with a bending modulus of 5.41 ± 1.14 kPa (WC) and 7.98 ± 2.22 kPa (AC).

Conclusions: The tri-layer scaffolds fabricated resemble the native aortic valve leaflets in structure and composition, and successfully introduced bending anisotropy in physiological conditions. Together with the suitable microstructure and promising mechanical properties, the design is reckoned to be a potential tissue engineering heart valve candidate.

Keywords

Type I atelocollagen, tissue engineering heart valve, tri-layer, bending anisotropy

Introduction

The heart of one of the most vital organs in the human body, yet it is susceptible to various valvular heart diseases (VHDs). In the United States, 8,250,000 people suffer from VHDs each year, which is approximately 2.5% of the country's population [1]. Among the adults diagnosed with VHDs, 75% of the cases involve malfunction in mitral or aortic valves [2]. Heart valve replacement is the main treatment, and over 300,000 valve replacement surgeries are performed annually around the world [3]. Clinically, 55% of valve replacement is mechanical valves and the rest 45% are bioprosthetic valves [4]. However successful, both types of valves are subjected to issues like thrombosis, low extensibility, immunogenic responses, calcification, and somatic growth incompatibility [5–7]. Tissue engineering, an emerging field combining biology and engineering, has been employed in the development of damage tissue replacement [8], and the use of extracellular matrix (ECM) materials is increasing in developing suitable scaffolds. Although constructing scaffolds using synthetic polymers such as polylactic acid (PLA) and polyglutamic acid (PGA) is being explored for advantages such as sufficient mechanical strength and the ability to biodegrade [9], natural polymers such as collagen, elastin, and glycosaminoglycans (GAGs) are preferred for their biocompatibility and great potential for both mechanical property and cellular response control.

The aortic valve leaflet is comprised of three layers: the fibrosa rich in collagen, the ventricularis situating elastin, and the spongiosa containing GAGs. Mechanically, the fibrosa serves as the main load bearer [10] while the ventricularis provides extensibility reaching 62% [11], and the middle spongiosa dampens shocks generated during the systole-diastole cycle and prevents delamination [12]. Structurally, the valve leaflets naturally bend towards the ventricularis side, and the bending resistance is different when the leaflet is bent facing a different direction illustrated in Figure 1 schematically. This bending anisotropy is crucial in regulating blood flow and preventing backflow, therefore is of great importance when developing tissue engineering heart valve scaffolds. Furthermore, a J-shaped stress-strain response to load is preferred (Figure 2), as the toe region and the transitional region allow the needed range of deformation physiologically in a reversible manner by the uncrimping and the slight slide of collagen fibres, and further deformation is limited in the linear region where greater stiffness is met with higher load, strengthening the structure against fracture [13]. Moreover, the reduced area under the stress-strain curves represents lowered energy stored that could lead to fracture of the material.

Collagen-based single-layer scaffolds have been studied extensively; however, they lack the effectiveness in mimicking the ECM structurally and mechanically [14, 15]. A few layered structures have been developed over the past decade based on natural polymers with bending anisotropy being reported, demonstrating the potential of collagen-based scaffolds in valve replacement [16–20]. Polymeric collagen with telopeptides, however, has been reported to be antigenic, and therefore is less biocompatible compared to its monomeric counterpart [21, 22]. Despite some applications in the osteochondral field, no tri-layer heart valve tissue engineering scaffold design based on atelocollagen has been studied before this study [23, 24].

Materials and methods

Scaffold fabrication

Type I atelocollagen (from bovine amnion, pepsin-digested, Memphis Veterans Affairs Medical Centre's Research Service, US), HA (hyaluronic acid, sodium salt, Thermo Fisher Scientific, US), and elastin (from bovine neck ligament, Merck Life Science Ltd, UK), were selected as scaffold materials. EDC hydrochloride (Thermo Fisher Scientific Ltd, UK) and NHS (Sigma-Aldrich Ltd, UK) were chosen as crosslinking agents.

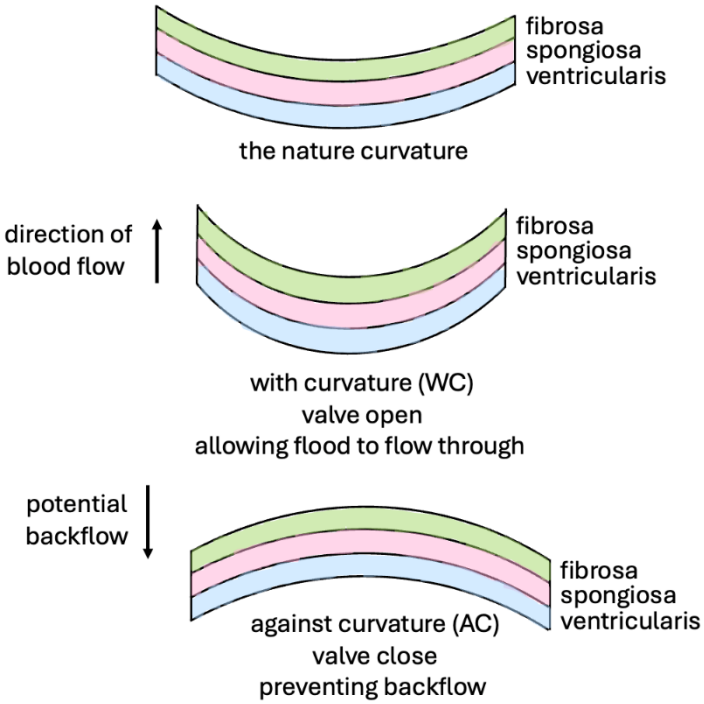

Figure 1. Schematic diagram of the bending anisotropy of native heart valve leaflet

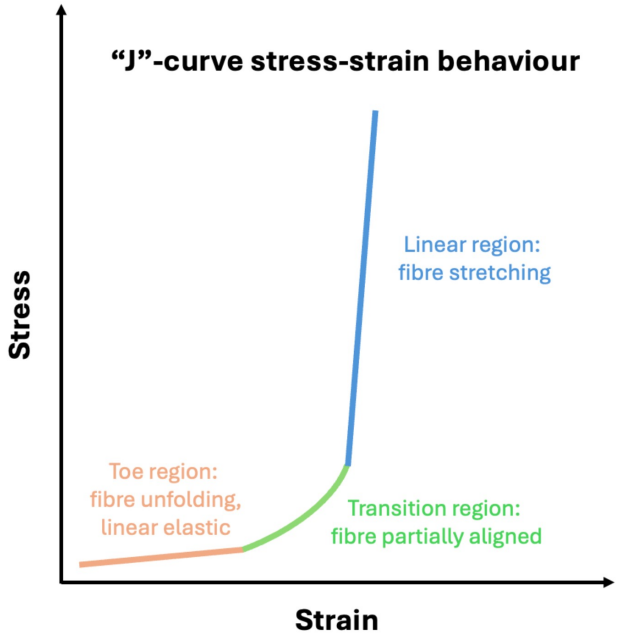

Figure 2. The J-curve stress-strain response of heart valve leaflets

Pepsin-digested collagen was first made into an aqueous solution to undergo fibrillogenesis. Lyophilised collagen was dispersed into 0.05 M acetic acid solution (pH 3.2) and subsequently added into tris-buffered saline (TBS, pH 7.6) of equal volume with gentle stirring. The pH of the mixture was adjusted to a physiological level, and the mixture was transferred to incubate at 37°C until the formation of collagen fibres [25].

EDC and NHS (ratio 2:1) were dissolved in acidic deionised water (pH 4.8). The fibrillar collagen suspension was poured into the crosslinking solution and left to react for 4 hours with gentle stirring. The mixture was then washed first with 1.0 M NaCl and then with deionised water to remove unreacted chemicals [26].

The crosslinked collagen suspension was cast into polytetrafluoroethylene (PTFE) moulds of various dimensions and frozen at –20°C overnight, and the frozen samples were freeze-dried in a Christ I-5 freeze-dryer (Martin Christ Gefriertrocknungsanlagen GmbH, Germany) for 24 hours under 5 Pa vacuum to obtain porous foam-like single-layer scaffolds.

The collagen-HA and elastin (in the form of fibrillar elastin gel) layers were prepared according to the previous studies [26]. Freeze-dried crosslinked collagen scaffolds were immersed in 0.4% wt adipic acid dihydrazide (ADH)-modified HA solution and the resultant HA-infiltrated collagen structure was washed before moulding. The fibrillar elastin gel used is a novel elastin developed within the group, it is a gel-formed elastin in between insoluble elastin and soluble α-elastin. To assemble the tri-layer structure, a multi-step casting method was adopted: A layer of collagen was loaded into the mould to one-third of the height, then a freshly washed pre-fabricated collagen-HA layer of equal thickness was gently placed on top, lastly the remaining one-third volume was filled with elastin gel. The entire structure was frozen at –20°C overnight and then freeze-dried to obtain porous tri-layer scaffolds.

Microstructure

The occurrence of fibrillogenesis was visualised using SEM (Zeiss), and the accelerating voltage was set at 5 kV. The collagen suspensions before and after fibrillogenesis induction were deposited onto aluminium pin stubs and left air-dry in a near vacuum before coating with platinum (Leica EM ACE600). The characteristic D-spacing pattern was analysed with ImageJ (National Institutes of Health, US).

The microstructure of the scaffolds was characterised by SEM (Zeiss) with the accelerating voltage being 10 kV. Samples were carefully sectioned into 1–2 mm slices using a sharp surgical scalpel and coated with 5 mm platinum. For single-layer scaffolds, samples were cross-sectioned; for tri-layer scaffolds, samples were sectioned along the axial plane to demonstrate the layered structure. For the pore morphology study, the pore area was assumed to be circular and analysed using ImageJ. The circularised pore diameter (d) was obtained with Equation 1, where A is the measured pore area.

$$d = 2\sqrt{\frac{A}{\pi}} \qquad \text{Equation 1}$$

Chemical structure

The chemical structure of the single-layer scaffolds was revealed by FTIR (Varian Excalibur FTS 3500 FT-IR Spectrometer) with the resolution and aperture setting being 4 cm^{-1} and 0.5 cm^{-1} at 2,000 cm^{-1}. The spectra obtained were processed and analysed using OriginLab.

Mechanical tests on non-hydrated scaffolds

Uniaxial compression tests were conducted on all scaffolds using a DMA Q800 (TA Instruments, US) at room temperature. The cylindrical samples (N = 5) were subjected to a 0.3 N/min force rate until 3 N was reached. Tensile and storage moduli mentioned supplementarily in the Discussion section were also obtained by DMA Q800. For viscoelasticity testing, the rectangular samples (N = 5) were subjected to 0.3 N preload and 0.1% constant strain under tension, with the tensile frequency oscillating at 0.1, 0.3, 1.0, 3.0, and 10.0 Hz. For tensile testing, the rectangular samples (N = 5) were subjected to a 0.3 N/min force rate similar to compressive testing until failure.

For tri-layer scaffolds, unidirectional three-point bend tests were performed using the DMA Q800 in both the WC (with curvature, sample bent towards the collagen layer) and the AC (against curvature, sample bent towards the elastin layer) directions. The rectangular samples (N = 5) were subjected to a 0.3 N/min force rate over a 20 mm span. Young's modulus was calculated from the slope of the linear elastic region of the resultant stress-strain curves.

Mechanical tests on hydrated scaffolds

An easy and adequately accurate "self-deflection" test was developed within the group and was further improved by the author to test the bending properties of the hydrated samples [17]. It is the method that

relies on linking the bending stiffness (EI, with E being the bending modulus and I being the second moment of inertia of a rectangular beam) to the maximum deflection (d_{max}) of the structure under uniformly distributed load (q) by the beam theory (Equation 2). In this method, the load is provided by the gravity of the phosphate-buffered saline (PBS) absorbed, which is expressed by the mass change/solution absorption before and after saturation. Figure 3 depicts the measurement of the maximum height (h) from the sample central plane to its lowest point and the sample thickness (t) to calculate d_{max} using Equation 3.

$$d_{max} = \frac{5ql^4}{384EI} \quad \text{Equation 2}$$

$$d = h - \frac{t}{2} \quad \text{Equation 3}$$

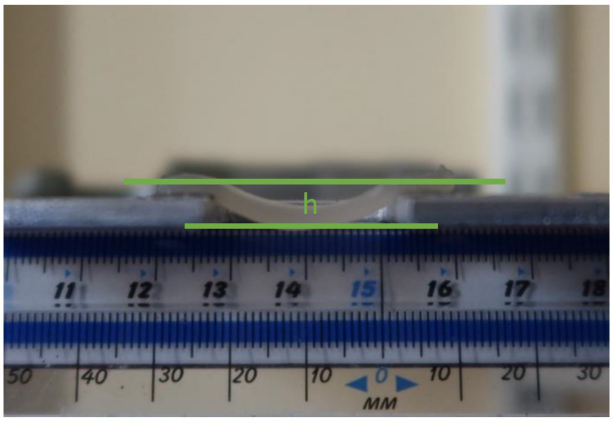

Figure 3. Picture of hydrated scaffold deflection measurement

The rectangular samples (N = 5) were pre-saturated with 0.1 M PBS at room temperature for an hour and then placed on a U-shaped metal plate with a span of 20 mm (l) to allow free deflection. With the mass of the sample being recorded before and after saturation, the mass change (Δm) was calculated, and the bending modulus can therefore be calculated using Equation 4, where g is the acceleration of gravity (9.8 m/s^2). The final equilibrium state of deflection was captured by a camera (Canon G7X Mark III, Japan) and the measurements were conducted using ImageJ. For tri-layer scaffolds, the tests were conducted in both the WC and AC directions.

$$E_{bend,wet} = \frac{5\Delta m g l^3}{384dI} \quad \text{Equation 4}$$

Uniaxial compression tests in the hydrated state were carried out only on tri-layer scaffolds due to limited resources. The test conditions were kept the same as the non-hydrated tests for direct comparison, and the hydration was achieved by testing the pre-saturated cylindrical samples in PBS submersion.

Results

Scanning electron microscopy

The atelocollagen was demonstrated to achieve fibrillogenesis successfully via the distinct fibre structure formation captured in Figure 4. The characteristic D-spacing pattern of collagen fibres was prominently displayed, and the spacing was measured to be 69.3 nm (N = 43), coinciding with the range (64–71 nm) reported in various literature [27–29].

Non-crosslinked scaffolds were not sufficiently stiff to be sectioned, hence only crosslinked collagen-only scaffolds were characterised. Scaffolds with a porosity of over 97% were successfully produced, meeting the tissue engineering requirement of 90% [30]. Figure 5 presents representative SEM images at

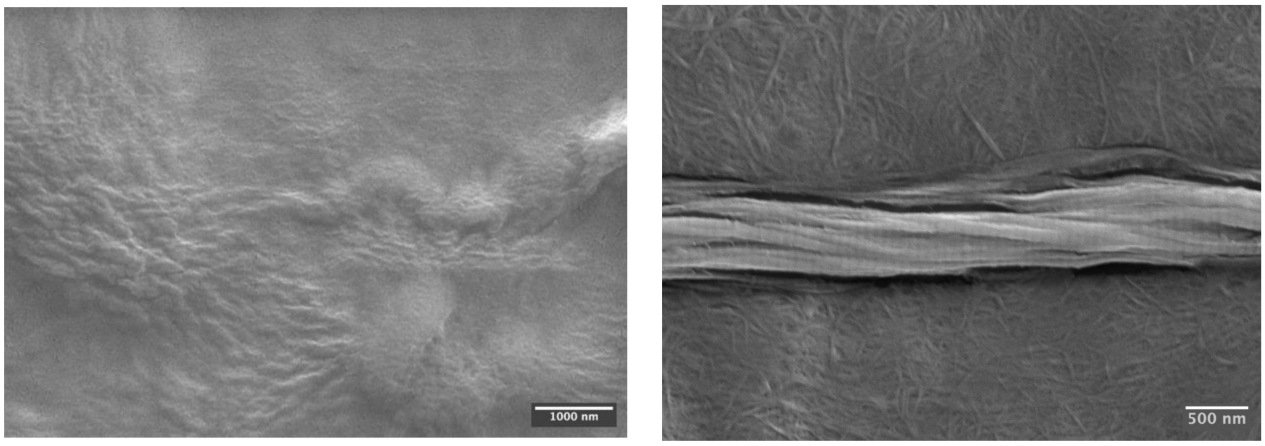

Figure 4. SEM images of the collagen suspension before (left) and after (right) fibrillogenesis. The left image shows no distinct fibre formation; in contrast, the right image demonstrates the fibrillar atelocollagen feature in the background and the characteristic D-spacing pattern on the middle fibre bundle formed after incubation

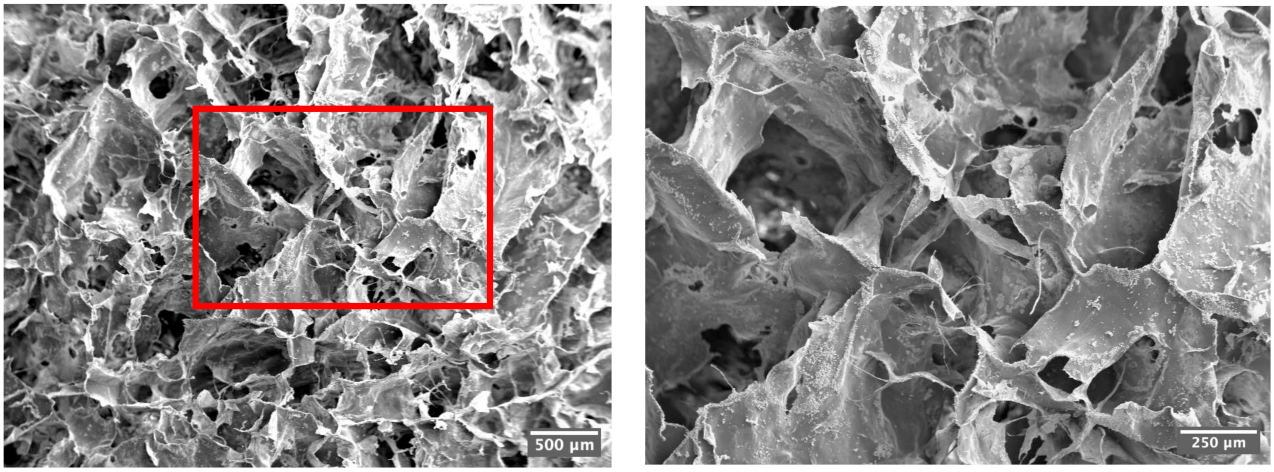

Figure 5. SEM images of the crosslinked collagen-only scaffolds under 20× (left) and 50× (right)

different magnifications of the collagen-only scaffolds, exhibiting desired interconnective and intact open pore morphology. Figure 6 showcases the seamless transitions between layers as well as the overview of three layers. Both mainly contain collagen, the layers collagen-only and collagen-HA show a subtle transition yet detectable by a change in the pore wall structure, i.e., the collagen-HA layer exhibits greater pore size (220 ± 142 µm) than the collagen-only layer (187 ± 83.0 µm) with less pore wall integrity and pore uniformity. The transition between the collagen-HA and elastin layer is more visibly marked by the flake-like feature of the elastin layer. The pore size of the collagen-only scaffolds was calculated to be 292 ± 41.4 µm with a wall thickness of 15.4 ± 4.40 µm. Interestingly, the average pore size of the collagen layer of the same making in the tri-layer structure, however, saw an approximate 40% decrease (187 ± 83.0 µm).

Fourier transform infrared spectroscopy

The FTIR spectra of the collagen scaffolds contained all five characteristic peaks of pure collagen, respectively, the amide A and B bands associated with N-H stretching, amide I signal resulted from C=O stretching and N-H bending, amide II peak containing N-H bending and C-N stretching signals, and the triplet peak amide III [31, 32]. It can be concluded that the fabrication method had no negative impact on the chemical backbone of collagen. Moreover, the amide III/1,450 cm^{-1} intensity ratio remained at ~1, indicating the preservation of the collagen triple helical structure [33].

Figure 7 presents the FTIR spectra of both non-crosslinked and crosslinked collagen scaffolds with normalisation against 2,930 cm^{-1}, which is a result of C-H stretching and is unaffected by EDC/NHS chemistry [34]. Both the amide I band at 1,633 cm^{-1} and the ester band at 1,161 cm^{-1} confirmed that the

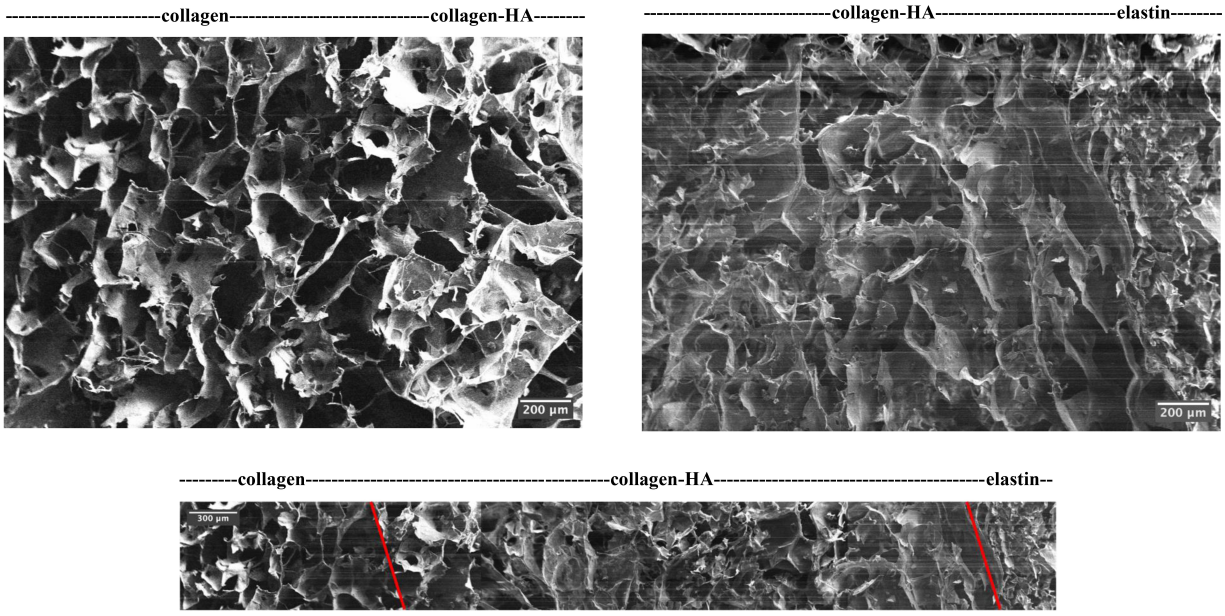

Figure 6. SEM images of the tri-layer scaffold interface between layers (top left and top right) and overview (bottom). The transition is marked by captions for the interfaces in the adjacent layers, and it is further indicated by the red lines in the overview* image. * Due to the section direction, the overview image could not be taken directly in one image and therefore is demonstrated by collaging five consecutive images. HA: hyaluronic acid

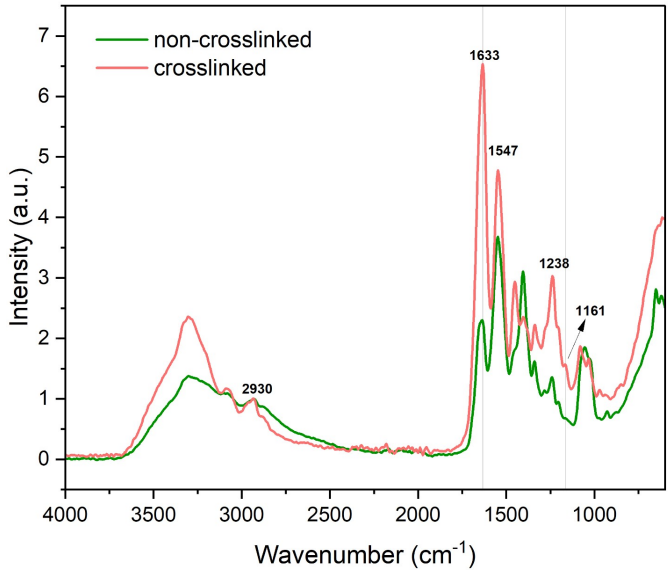

Figure 7. FTIR spectra of non-crosslinked and crosslinked collagen scaffolds normalised against 2,930 cm^{-1}. a.u.: absorbance unit

crosslinking chemistry was effective and unharmful to the collagen backbone structure [35, 36]. The relative crosslinking extent was further studied to examine the contributions of the amide and ester bonds by comparing the relative intensity before and after crosslinking, and the result is visualised in Figure 8. After partial crosslinking, the amide bond intensity saw a 1.9 times improvement. In comparison, the ester bond intensity increased by 1.3 times, indicating that the amide bond played the leading role in the EDC/NHS crosslinking chemistry of collagen.

Compressive properties

In the non-hydrated state, EDC/NHS crosslinking was demonstrated to have a positive impact on the compressive stiffness of collagen-only scaffolds, with a 1.4-fold improvement in the compressive modulus (from 29.1 ± 4.24 kPa to 39.7 ± 1.68 kPa). It can be observed from Figure 9 that both the collagen-only and tri-layer scaffolds shared the stress-strain curve features of lightly crosslinked polymers, with the stress

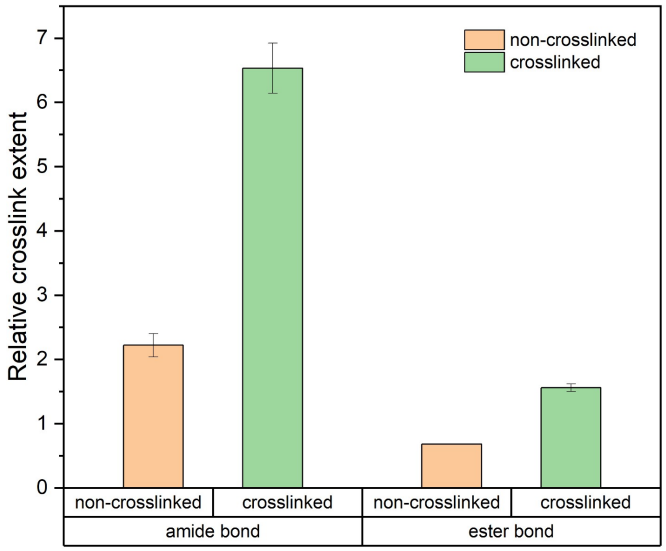

Figure 8. The relative crosslinking extent of amide bonds (1,633 cm^{-1}/2,930 cm^{-1}) and ester bonds (1,161 cm^{-1}/2,930 cm^{-1}) of the collagen scaffolds before and after EDC/NHS partial crosslinking. The results are shown as the average value with the error bar demonstrating the standard deviation*. * The error bar is missing for the ester bond intensity of non-crosslinked samples as it was calculated to be zero

plateau showing a noticeably positive slope. The compressive behaviour of the other two layers was characterised outside of the scope of this paper but included for comparison. It can be interpreted from the curves that the much stiffer collagen-HA layer and elastin layer mainly contribute to the stiffness of the tri-layer structure, in other words, the addition of the two layers increased compression resistance, resulting in a compressive modulus of 112 ± 32.9 kPa.

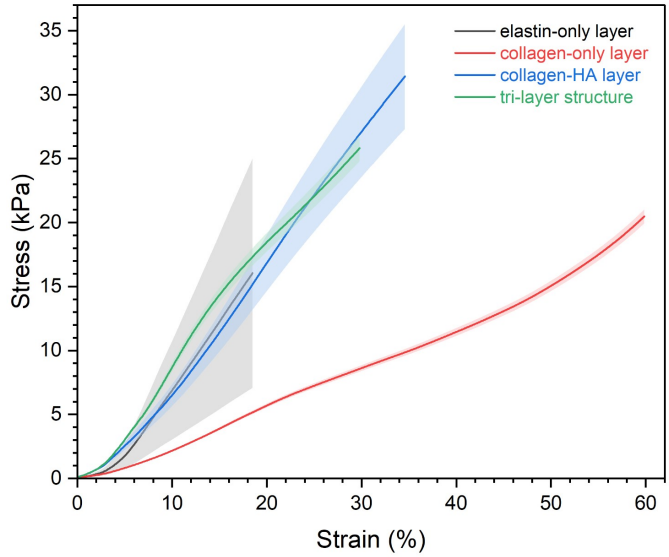

Figure 9. Compressive stress-strain curves of the tri-layer scaffold and its single component layers in the non-hydrated state. The shadowed area represents the standard deviation

J-curve deformation is preferred because it allows the structure the flexibility to undergo normal physiological movement and the deformation resistance when excessive force is applied. After hydration, the tri-layer scaffolds exhibited a J-shaped stress-strain response under compression (Figure 10), confirming the biomedical potential of the design. Hydration effectively extended the linear region from 12% strain to 45% strain; however, it drastically reduced the compressive stiffness (expressed by Young's modulus) from 112 ± 32.9 kPa to 0.907 ± 0.0434 kPa.

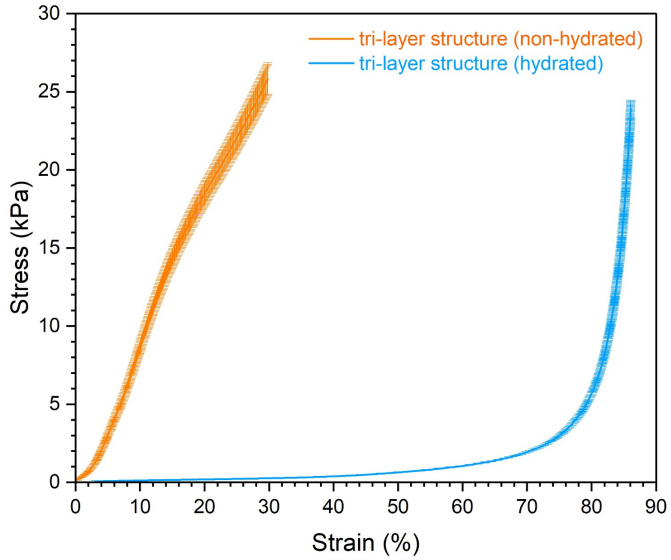

Figure 10. Compressive stress-strain curves of the tri-layer scaffold in the non-hydrated and hydrated states (shown as average with error bars indicating the standard deviation)

Bending properties

According to Equations 2 and 3, the hydrated bending modulus of the collagen-only scaffold was calculated to be 6.46 ± 1.15 kPa. The theoretical bending modulus in the non-hydrated state was calculated to be ~135 kPa using the preliminary tensile and compressive moduli obtained from experiments. It can be seen that hydration drastically reduced scaffold stiffness; however, it is still deemed ideal for that softer matrix (~6–14 kPa) is reported to better suit cell seeding [9].

For tri-layer scaffolds, the bending response was examined in both WC and AC directions due to the layered nature of the designs. The scaffolds are expected to be stiffer and more bending-resistant in the AC direction to effectively prevent blood backflow and the stronger compression resistance of elastin compared to collagen is predicted to help achieve that. The results of the bending moduli are organised in Table 1. It can be seen that in both non-hydrated and hydrated states, the scaffolds are stiffer in the AC direction, coinciding with the anisotropicity discovered in native heart valve leaflets [17]. The results again confirmed that hydration reduces scaffold stiffness by a great amount, in this case, 95 %.

Table 1. Summary of the bending modulus of tri-layer scaffolds in both non-hydrated and hydrated states

States	E_{bend} (kPa) in WC direction	E_{bend} (kPa) in AC direction
Non-hydrated	1,210 ± 178	1,450 ± 392
Hydrated	5.41 ± 1.14	7.98 ± 2.22

The tests were conducted in both WC and AC directions. Results are presented as average ± standard deviation. AC: against curvature; WC: with curvature

Discussion

Crosslinking is expected to improve the scaffold stiffness. Other than introducing smaller pore sizes, crosslinking has a direct impact on Young's modulus. According to the rubber elasticity theory [37], the effective crosslinking density (v_e) is linearly dependent on Young's modulus (E) when under the same temperature (T) with the same volume fraction (Φ), which can be expressed using Equation 5, with R being the gas constant.

$$V_e = \frac{E\emptyset^{-\frac{1}{3}}}{3RT} \quad \text{Equation 5}$$

After partially crosslinked with EDC/NHS, the compressive modulus in the non-hydrated state increased by 40%, which should coincide with the crosslinking density increment. However, from the FTIR intensity study, this value is largely under the relative crosslinking extent. This inconsistency is explained by the possibility that not all amide and ester bonds formed contributed to the effective crosslink density. It is also worth mentioning that the commonly used method to characterise polymer crosslinking density, the swelling test, is not adopted in this study. The reason lies in the fact that crosslinking density is only one of the factors that contribute to the swelling ability of porous collagenous structures. Other factors include but are not limited to collagen concentration [38], solvent type [39], fabrication method and fibre alignment [40], pore morphology [41], and ambient temperature and pressure. The commonly conducted free amino acid analysis [42] or 2,4,6-trinitrobenzene sulfonic acid (TNBS) assay [43] is recommended for potential future work. Still, crosslinking is seen to effectively improve the mechanical properties, with the storage modulus, compressive modulus, and tensile modulus experiencing a 1.1-fold (from 2.43 ± 0.24 MPa to 2.77 ± 0.55 MPa), 1.4-fold (from 29.1 ± 4.24 kPa to 39.7 ± 1.68 kPa), and 1.6-fold (from 1.14 ± 0.118 MPa to 1.77 ± 0.364 MPa) increase respectively.

A few possible explanations were proposed to explain the average pore size discrepancy between the collagen-only scaffold and the collagen-only layer within the tri-layer structure. Batch-to-batch differences and the slight compression to the bottom layer during sample sectioning can partially contribute to the problem yet are deemed trivial. The compression of the bottom layer during the moulding process is hypothesised to be the main reason behind the reduced pore size. The flattening technique involves gently tapping the loaded moulds on a flat surface to allow an even distribution of the highly viscous suspension, which poses no problem in homogenous constituent scaffold production. However, elastin with a much greater density (~0.083 g/cm^3, collagen suspension density is ~0.006 g/cm^3) will inevitably impose a downward-facing force on the bottom layer when it is moulded, while the bottom collagen layer has less structure stiffness (Young's modulus 1.03 kPa based on preliminary results) and a shear-thinning nature. To address this issue, the elastin layer was first moulded, yet the extremely high viscosity was proven to be an obstacle to obtaining the flat surface necessary for subsequent layer addition. It is also worth mentioning that the low thermal conductivity of the PTFE moulds used hindered the volumetric freezing process, and the expanding surface layer exerted an extra compressive force towards the bottom collagen layer.

The characteristic compressive stress-strain curve of elastomeric foams is often divided into three segments, i.e., the elastic region, the stress plateau, and the densification region. The linear elastic region is the result of pore edge bending while the stress plateau is attributed to pore wall buckling, and pore collapsing contributes to the densification [44]. From Figure 9 it can be seen that the stress plateau of both collagen-only and tri-layer scaffolds was presented as a linear region with elevated slope. This variation is attributed to the various pore sizes and wall thickness. A linear dependence of plateau strain exists on pore dimensions and a cubic dependence on wall thickness, and given the observed spread in both values, the non-ideal compression response can be easily explained. Several studies mentioned strain hardening and non-Gaussian stretching as possible mechanisms [45–48], yet based on the above observations and explanations, it is highly unlikely that strain hardening could be a mechanism in this case. Hydration was shown to greatly alter the stress-strain curve shape and reduce scaffold stiffness. The different deformation pattern is attributed to the change in lubrication and the resultant molecular interaction. With water molecules, the naturally crimped collagen fibres can unfold and align macroscopically [13]. With slightly more stress, further chain movement is facilitated by water molecules, allowing the linear elastic region to be extended compared to the non-hydrated system [49]. This unique deformation mechanism allows extreme structure flexibility when the device is placed in a dynamic flow, and once the load exceeds normality, the structure can toughen up and respond by entering the densification region where the collagen fibre elasticity is restricted by hydrogen bonds [50]. The drastic drop in compressive modulus after hydration was reported in various studies [51–54]. Instead of applying the Flory-Rehner model, which is limited by entropic elasticity [55], a scaling law theory can better explain the experimental data, where the hydrated compressive modulus has a 2.3 power law relationship with the non-hydrated modulus [56].

The bending anisotropy obtained is essential for heart valve tissue engineering. During a cardiac cycle, the ventricle contraction (systole) pumps the blood from the left ventricle into the aorta, forcing the valves to open; later, while the left ventricle experiences a relaxation process (diastole), the valves close to prevent blood backflow [57]. To achieve these movements, it is required that the valves be stiffer in the AC direction and able to withstand the blood pressure in diastole [58]. The layered structure provided a potential route to achieve this desired property. Bending is equivalent to a combination of compression and tension on either side of the neutral axis. When the structure is placed in the WC direction, the collagen-only fibrosa-mimicking layer is theoretically under compression while the elastin-only ventricularis-resembling layer would be under tension, and vice versa in the AC direction. The neutral axis plane was calculated to be located at ~14% of the total scaffold thickness from the bottom, in other words, the elastin layer is only partially under tension in the WC bending direction and the collagen layer partially in the AC direction and the bending deformation is compression-dominant. The collagen-only layer is demonstrated to be less compression-resistant, therefore, the tri-layer structure is expected to be less stiff in the WC direction. It is worth mentioning that due to limited resources, the hydrated mechanical properties of individual layers were unable to be investigated. It is highly recommended by the author for future work to further understand the contribution of each layer and the mechanical response of the design under physiological circumstances.

With the microstructure and mechanical properties being the focus, the potential of this design as a heart valve tissue engineering candidate is examined. Despite the asymmetrical pores with varying sizes, the scaffold microstructure is still deemed to favour cell activities of both the valvular endothelial cells and interstitial cells based on their ability to alter their shape and size in response to the blood flow pattern, the valve curvature, and the physiological shear stress distribution [59]. The average pore size reported in this study falls under the upper limit where cells would fail to colonise the structure due to limited bridging and networking with adjacent cells [60] and above the lower threshold of cell viability [61]. Scaffolds with similar structure and composition were extensively studied within the author's group and despite the absence of cell work in this study, one previous research has demonstrated proven feasibility for *in vitro* and *in vivo* studies of the design [62]. In the aspect of mechanical strength, this design showed a largely improved hydrated compressive modulus compared to similar structures with a reported value of ~3.5 Pa [63]. The bending stiffness of the native human aortic valve leaflets was characterised in various studies [64, 65], and while it may seem that the scaffolds made in this study are less mechanically sufficient, it is hypothesised that with the increase in collagen percentage and crosslinking density, together with the cells' ability to regulate and enhance the flexure resistance [18], the design still provides a potential platform for development for future collagen-based heart valve tissue engineering scaffold studies.

Conclusions

This study has successfully fabricated and characterised the proposed tri-layer scaffold design with type I atelocollagen, HA, and fibrillar elastin gel. The design closely mimicked the tri-layer structure of the native aortic valves, and the bending anisotropy was successfully introduced. The proposed fabrication method, freeze-drying, and the crosslinking chemistry, EDC/NHS partial crosslink, were proven to be effective while able to preserve the collagen backbone structure. The design demonstrated a suitable microstructure for cell-related activities with varying pore sizes and interconnected pores. Under physiological conditions, the structure experienced the desired J-shaped curve under compression. Overall, the proposed tri-layer scaffold design showed potential for future developments as a tissue engineering heart valve.

Abbreviations

AC: against curvature

FITR: Fourier transform infrared spectroscopy

HA: hyaluronic acid

PBS: phosphate-buffered saline

VHDs: valvular heart diseases

WC: with curvature

Declarations

Acknowledgement

The authors would like to thank Nick Hawkins and the Thermal Mechanical Lab in the Department of Engineering, University of Oxford for the mechanical testing equipment and assistance.

Author contributions

ZM: Conceptualization, Investigation, Writing—original draft, Writing—review & editing. RJS: Investigation. DDB: Resources. JTC: Validation, Writing—review & editing, Supervision. All authors read and approved the submitted version.

Conflicts of interest

The authors declare that they have no conflicts of interest.

Ethical approval

Not applicable.

Consent to participate

Not applicable.

Consent to publication

Not applicable.

Availability of data and materials

The raw data supporting the conclusions of this manuscript is available upon enquiry at zhaoying.ma@materials.ox.ac.uk without undue reservation, by any qualified researcher.

Funding

Not applicable.

References

1. Nkomo VT, Gardin JM, Skelton TN, Gottdiener JS, Scott CG, Enriquez-Sarano M. Burden of valvular heart diseases: a population-based study. Lancet. 2006;368:1005–11. [DOI] [PubMed]
2. Saurav A, Alla VM, Kaushik M, Hunter CC, Mooss AV. Outcomes of mitral valve repair compared with replacement in patients undergoing concomitant aortic valve surgery: a meta-analysis of observational studies. Eur J Cardiothorac Surg. 2015;48:347–53. [DOI] [PubMed]
3. Kheradvar A, Groves EM, Dasi LP, Alavi SH, Tranquillo R, Grande-Allen KJ, et al. Emerging trends in heart valve engineering: Part I. Solutions for future. Ann Biomed Eng. 2015;43:833–43. [DOI] [PubMed]
4. Fioretta ES, Dijkman PE, Emmert MY, Hoerstrup SP. The future of heart valve replacement: recent developments and translational challenges for heart valve tissue engineering. J Tissue Eng Regen Med. 2018;12:e323–35. [DOI] [PubMed]
5. Oveissi F, Naficy S, Lee A, Winlaw DS, Dehghani F. Materials and manufacturing perspectives in engineering heart valves: a review. Mater Today Bio. 2019;5:100038. [DOI] [PubMed] [PMC]

6. Alsoufi B. Aortic valve replacement in children: Options and outcomes. J Saudi Heart Assoc. 2014;26:33–41. [DOI] [PubMed] [PMC]
7. Nishimura RA, Warnes CA. Anticoagulation during pregnancy in women with prosthetic valves: evidence, guidelines and unanswered questions. Heart. 2015;101:430–5. [DOI] [PubMed]
8. Langer R, Vacanti JP. Tissue engineering. Science. 1993;260:920–6. [DOI] [PubMed]
9. Hinderer S, Seifert J, Votteler M, Shen N, Rheinlaender J, Schäffer TE, et al. Engineering of a bio-functionalized hybrid off-the-shelf heart valve. Biomaterials. 2014;35:2130–9. [DOI] [PubMed]
10. Vesely I, Noseworthy R. Micromechanics of the fibrosa and the ventricularis in aortic valve leaflets. J Biomech. 1992;25:101–13. [DOI] [PubMed]
11. Lee JM, Boughner DR, Courtman DW. The glutaraldehyde-stabilized porcine aortic valve xenograft. II. Effect of fixation with or without pressure on the tensile viscoelastic properties of the leaflet material. J Biomed Mater Res. 1984;18:79–98. [DOI] [PubMed]
12. Vyavahare N, Ogle M, Schoen FJ, Zand R, Gloeckner DC, Sacks M, et al. Mechanisms of bioprosthetic heart valve failure: fatigue causes collagen denaturation and glycosaminoglycan loss. J Biomed Mater Res. 1999;46:44–50. [DOI] [PubMed]
13. Robi K, Jakob N, Matevz K, Matjaz V. The Physiology of Sports Injuries and Repair Processes. In: Hamlin M, Draper N, Kathiravel Y, editors. Current Issues in Sports and Exercise Medicine. IntechOpen; 2013. [DOI]
14. Sachlos E, Reis N, Ainsley C, Derby B, Czernuszka JT. Novel collagen scaffolds with predefined internal morphology made by solid freeform fabrication. Biomaterials. 2003;24:1487–97. [DOI] [PubMed]
15. Salvatore L, Calò E, Bonfrate V, Pedone D, Gallo N, Natali ML, et al. Exploring the effects of the crosslink density on the physicochemical properties of collagen-based scaffolds. Polym Test. 2021;93:106966. [DOI]
16. Chen Q, Bruyneel A, Carr C, Czernuszka J. Bio-mechanical properties of novel bi-layer collagen-elastin scaffolds for heart valve tissue engineering. Procedia Eng. 2013;59:247–54. [DOI]
17. Chen Q, Bruyneel A, Carr C, Czernuszka J. Trilayer scaffold with cardiosphere-derived cells for heart valve tissue engineering. J Biomed Mater Res B Appl Biomater. 2020;108:729–37. [DOI] [PubMed]
18. Nazir R, Bruyneel A, Carr C, Czernuszka J. Collagen type I and hyaluronic acid based hybrid scaffolds for heart valve tissue engineering. Biopolymers. 2019;110:e23278. [DOI] [PubMed]
19. Nazir R, Bruyneel A, Carr C, Czernuszka J. Mechanical and Degradation Properties of Hybrid Scaffolds for Tissue Engineered Heart Valve (TEHV). J Funct Biomater. 2021;12:20. [DOI] [PubMed] [PMC]
20. Merryman WD, Huang HS, Schoen FJ, Sacks MS. The effects of cellular contraction on aortic valve leaflet flexural stiffness. J Biomech. 2006;39:88–96. [DOI] [PubMed]
21. Lynn AK, Yannas IV, Bonfield W. Antigenicity and immunogenicity of collagen. J Biomed Mater Res B Appl Biomater. 2004;71:343–54. [DOI] [PubMed]
22. Miyata T, Taira T, Noishiki Y. Collagen engineering for biomaterial use. Clin Mater. 1992;9:139–48. [DOI] [PubMed]
23. Abbasi N, Hamlet S, Love RM, Nguyen NT. Porous scaffolds for bone regeneration. J Sci Adv Mater Devices. 2020;5:1–9. [DOI]
24. Lien S, Ko L, Huang T. Effect of pore size on ECM secretion and cell growth in gelatin scaffold for articular cartilage tissue engineering. Acta Biomater. 2009;5:670–9. [DOI] [PubMed]
25. Rashidi N. Fabrication of a Novel Bilayered Osteochondral Scaffold Using a Bottom up Approach [dissertation]. Oxford: Oxford University; 2018.
26. Iftekhar S. Isolation of Fibrillar Elastin Gel (FEG) and its application in heart valve tissue engineering [dissertation]. Oxford: Oxford University; 2020.
27. Baer E, Cassidy JJ, Hiltner A. Hierarchical Structure of Collagen Composite Systems. In: Glasser WG, Hatakeyama H, editors. Viscoelasticity of Biomaterials. American Chemical Society; 1992. pp. 2–23. [DOI]

28. Bozec L, van der Heijden G, Horton M. Collagen fibrils: nanoscale ropes. Biophys J. 2007;92:70–5. [DOI] [PubMed] [PMC]
29. Borrego-González S, Rico-Llanos G, Becerra J, Díaz-Cuenca A, Visser R. Sponge-like processed D-periodic self-assembled atelocollagen supports bone formation in vivo. Mater Sci Eng C Mater Biol Appl. 2021;120:111679. [DOI] [PubMed]
30. Wu Y, Lee T, Chiu K, Shaw S, Yang C. A comparative study of the physical and mechanical properties of three natural corals based on the criteria for bone-tissue engineering scaffolds. J Mater Sci Mater Med. 2009;20:1273–80. [DOI] [PubMed]
31. Stani C, Vaccari L, Mitri E, Birarda G. FTIR investigation of the secondary structure of type I collagen: New insight into the amide III band. Spectrochim Acta A Mol Biomol Spectrosc. 2020;229:118006. [DOI] [PubMed]
32. Ji Y, Yang X, Ji Z, Zhu L, Ma N, Chen D, et al. DFT-Calculated IR Spectrum Amide I, II, and III Band Contributions of *N*-Methylacetamide Fine Components. ACS Omega. 2020;5:8572–8. [DOI] [PubMed] [PMC]
33. Machado AAS, Martins VCA, Plepis AMG. Thermal and rheological behavior of collagen: Chitosan blends. J Therm Anal Calorim. 2002;67:491–8. [DOI]
34. Lee Y, Chiang C, Huang P, Chung C, Huang TD, Wang C, et al. Evidence of preserved collagen in an Early Jurassic sauropodomorph dinosaur revealed by synchrotron FTIR microspectroscopy. Nat Commun. 2017;8:14220. [DOI] [PubMed] [PMC]
35. Wang XH, Li DP, Wang WJ, Feng QL, Cui FZ, Xu YX, et al. Crosslinked collagen/chitosan matrix for artificial livers. Biomaterials. 2003;24:3213–20. [DOI] [PubMed]
36. Schmidt FN, Zimmermann EA, Campbell GM, Sroga GE, Püschel K, Amling M, et al. Assessment of collagen quality associated with non-enzymatic cross-links in human bone using Fourier-transform infrared imaging. Bone. 2017;97:243–51. [DOI] [PubMed] [PMC]
37. Peppas NA, Merrill EW. Crosslinked poly(vinyl alcohol) hydrogels as swollen elastic networks. J Appl Polym Sci. 1977;21:1763–70. [DOI]
38. Takallu S, Mirzaei E, Azadi A, Karimizade A, Tavakol S. Plate-shape carbonated hydroxyapatite/collagen nanocomposite hydrogel via in situ mineralization of hydroxyapatite concurrent with gelation of collagen at pH = 7.4 and 37°C. J Biomed Mater Res B Appl Biomater. 2019;107:1920–9. [DOI] [PubMed]
39. Lai VK, Nedrelow DS, Lake SP, Kim B, Weiss EM, Tranquillo RT, et al. Swelling of Collagen-Hyaluronic Acid Co-Gels: An In Vitro Residual Stress Model. Ann Biomed Eng. 2016;44:2984–93. [DOI] [PubMed] [PMC]
40. Tonndorf R, Gossla E, Aibibu D, Lindner M, Gelinsky M, Cherif C. Wet spinning and riboflavin crosslinking of collagen type I/III filaments. Biomed Mater. 2018;14:015007. [DOI] [PubMed]
41. Monfregola L, Bugatti V, Amodeo P, De Luca S, Vittoria V. Physical and water sorption properties of chemically modified pectin with an environmentally friendly process. Biomacromolecules. 2011;12:2311–8. [DOI] [PubMed]
42. Grover CN, Gwynne JH, Pugh N, Hamaia S, Farndale RW, Best SM, et al. Crosslinking and composition influence the surface properties, mechanical stiffness and cell reactivity of collagen-based films. Acta Biomater. 2012;8:3080–90. [DOI] [PubMed] [PMC]
43. Madaghiele M, Calò E, Salvatore L, Bonfrate V, Pedone D, Frigione M, et al. Assessment of collagen crosslinking and denaturation for the design of regenerative scaffolds. J Biomed Mater Res A. 2016;104:186–94. [DOI] [PubMed]
44. Harley BA, Leung JH, Silva ECCM, Gibson LJ. Mechanical characterization of collagen-glycosaminoglycan scaffolds. Acta Biomater. 2007;3:463–74. [DOI] [PubMed]
45. Xu Y, Šavija B. 3D auxetic cementitious-polymeric composite structure with compressive strain-hardening behavior. Eng Struct. 2023;294:116734. [DOI]

46. Xu D, Craig SL. Strain Hardening and Strain Softening of Reversibly Cross-linked Supramolecular Polymer Networks. Macromolecules. 2011;44:7478–88. [DOI] [PubMed] [PMC]
47. Liao T, Yang X, Zhao X, Tang Y, Jiang Z, Men Y. Gaussian and Non-Gaussian Distributions of Fracture Properties in Tensile Stretching of High-Density Polyethylene. Macromolecules. 2021;54:8860–74. [DOI]
48. Zhao JH, Xie ZL, Zhong T, Sun T, Fezzaa K, Cai Y, et al. Strain rate effects on the mechanical behavior of porous titanium with different pore sizes. Mater Sci Eng A. 2021;821:141593. [DOI]
49. Pissis P, Kyritsis A. Hydration studies in polymer hydrogels. J Polym Sci Part B Polym Phys. 2013;51:159–75. [DOI]
50. Huang Y, Li X, Lu Z, Zhang H, Huang J, Yan K, et al. Nanofiber-reinforced bulk hydrogel: preparation and structural, mechanical, and biological properties. J Mater Chem B. 2020;8:9794–803. [DOI] [PubMed]
51. Suchý T, Šupová M, Bartoš M, Sedláček R, Piola M, Soncini M, et al. Dry versus hydrated collagen scaffolds: are dry states representative of hydrated states? J Mater Sci Mater Med. 2018;29:20. [DOI] [PubMed]
52. Varley MC, Neelakantan S, Clyne TW, Dean J, Brooks RA, Markaki AE. Cell structure, stiffness and permeability of freeze-dried collagen scaffolds in dry and hydrated states. Acta Biomater. 2016;33:166–75. [DOI] [PubMed]
53. Davidenko N, Schuster CF, Bax DV, Raynal N, Farndale RW, Best SM, et al. Control of crosslinking for tailoring collagen-based scaffolds stability and mechanics. Acta Biomater. 2015;25:131–42. [DOI] [PubMed] [PMC]
54. Wang X, Li Q, Hu X, Ma L, You C, Zheng Y, et al. Fabrication and characterization of poly(L-lactide-co-glycolide) knitted mesh-reinforced collagen-chitosan hybrid scaffolds for dermal tissue engineering. J Mech Behav Biomed Mater. 2012;8:204–15. [DOI] [PubMed]
55. Xu S, Zhou Z, Liu Z, Sharma P. Concurrent stiffening and softening in hydrogels under dehydration. Sci Adv. 2023;9:eade3240. [DOI] [PubMed] [PMC]
56. Li Z, Liu Z, Ng TY, Sharma P. The effect of water content on the elastic modulus and fracture energy of hydrogel. Extrem Mech Lett. 2020;35:100617. [DOI]
57. Pelech AN. Murmurs. In: Kliegman RM, Lye PS, Bordini BJ, Toth H, Basel D, editors. Nelson Pediatric Symptom-Based Diagnosis. Elsevier; 2018. pp. 116–43.e2. [DOI]
58. Calvert JW, Lefer DJ. Chapter 6 - Overview of Cardiac Muscle Physiology. In: Hill JA, Olson EN, editors. Academic Press; 2012. pp. 57–66. [DOI]
59. Butcher JT, Nerem RM. Valvular endothelial cells and the mechanoregulation of valvular pathology. Philos Trans R Soc Lond B Biol Sci. 2007;362:1445–57. [DOI] [PubMed] [PMC]
60. Salem AK, Stevens R, Pearson RG, Davies MC, Tendler SJB, Roberts CJ, et al. Interactions of 3T3 fibroblasts and endothelial cells with defined pore features. J Biomed Mater Res. 2002;61:212–7. [DOI] [PubMed]
61. Yannas IV, Lee E, Orgill DP, Skrabut EM, Murphy GF. Synthesis and characterization of a model extracellular matrix that induces partial regeneration of adult mammalian skin. Proc Natl Acad Sci U S A. 1989;86:933–7. [DOI] [PubMed] [PMC]
62. Gezmis H. The influence of collagen-based scaffolds on cardiac differentiation and endothelial growth [dissertation]. Oxford: Oxford University; 2023.
63. Cao R, Xu Y, Xu Y, Brand DD, Zhou G, Xiao K, et al. Development of Tri-Layered Biomimetic Atelocollagen Scaffolds with Interfaces for Osteochondral Tissue Engineering. Adv Healthc Mater. 2022;11:e2101643. [DOI] [PubMed]
64. Brazile B, Wang B, Wang G, Bertucci R, Prabhu R, Patnaik SS, et al. On the bending properties of porcine mitral, tricuspid, aortic, and pulmonary valve leaflets. J Long Term Eff Med Implants. 2015;25:41–53. [DOI] [PubMed] [PMC]

65. Lam TV. The Mechanical Properties of Native Porcine Aortic and Pulmonary Heart Valve Leaflets [dissertation]. Pittsburgh: University of Pittsburgh; 2005.